Exchange interactions and Curie temperatures in $Ni_{2-x}MnSb$ alloys: First-principles study

J. Rusz,[1,*,†] L. Bergqvist,[2] J. Kudrnovský,[3] and I. Turek[1,‡]
[1]*Department of Electronic Structures, Faculty of Mathematics and Physics, Charles University, Ke Karlovu 5, 121 16 Prague 2, Czech Republic*
[2]*Department of Physics, Uppsala University, Box 530, 751 21 Uppsala, Sweden*
[3]*Institute of Physics, Academy of Sciences of the Czech Republic, Na Slovance 2, 182 21 Prague 8, Czech Republic*
(Received 16 March 2005; revised manuscript received 1 March 2006; published 7 June 2006)

We present a first-principles study of the physical properties of the disordered $Ni_{2-x}MnSb$ alloys which form a continuous series connecting two typical members of the Heusler alloy family: namely, the half-metallic semi-Heusler alloy NiMnSb ($x=1$) and related metallic Heusler alloy Ni_2MnSb ($x=0$). Magnetic moments, exchange interactions, magnon spectra, and Curie temperatures at ambient and elevated pressures are determined and compared with available experimental data. The spin-spin correlation functions at the critical temperature are also calculated. The pair exchange interactions and corresponding classical Heisenberg Hamiltonian are derived from self-consistent electronic structure calculations using a magnetic force theorem. Heusler alloys NiMnSb and Ni_2MnSb exhibit strikingly different asymptotic behavior of exchange interactions with the distance between magnetic atoms. The Curie temperatures are estimated using multisublattice versions of the mean-field approximation, random-phase approximation, and Monte Carlo simulations. The robustness of the results with respect to the effect of correlations beyond the local density approximation, the selected reference state used for mapping to the Heisenberg Hamiltonian, and the applied mapping procedure are also discussed.

DOI: 10.1103/PhysRevB.73.214412 PACS number(s): 75.30.Et, 75.50.Gg

I. INTRODUCTION

The evaluation of the finite-temperature properties of complex materials on an *ab initio* level remains a challenge for solid-state theory. In recent years, interest in model Hamiltonians has been increasing due to the possibility to obtain values of their parameters from modern parameter-free theories of the electronic structure of solids based on density functional theory[1] in the framework of the local spin-density approximation (LSDA). An enormous growth of computer power allows one to obtain realistic parameters for complex materials with a reasonable effort. The finite-temperature study of such model Hamiltonians can be then done using sophisticated statistical methods. This two-step approach has been used by a number of authors also for the finite-temperature properties of magnetic materials studied in the framework of the classical Heisenberg Hamiltonian.[2–13] The concept of local magnetic moments in such magnetic systems is justified by the adiabatic approximation[2,14] valid in particular for systems with well-developed magnetic moments like, e.g., Mn and Fe.

Most of such studies were, however, related to systems with a simple lattice[2–4,10] or to systems with magnetic moments relevant just on one of the sublattices of a complex lattice.[6,8,9,13] The Heusler-type alloys represent an example of a magnetic system with the complex lattice and with well-documented physical properties, including transition temperatures. Very recently the exchange interactions and Curie temperatures of some Heusler alloys have been calculated.[5,11–13] The authors of Refs. 5, 12, and 13 used frozen-magnon calculations in the framework of the generalized gradient approximation (GGA) to extract exchange interactions while direct evaluation of such interactions in real space[2,15] was used in Ref. 11. The transition temperatures of the resulting classical Heisenberg Hamiltonian were then estimated in the framework of the mean-field approximation (MFA), and good agreement with experimental results has been obtained. This is surprising due to the fact that in previous studies the MFA values usually overestimated the experimental critical temperatures.

It is the main purpose of this paper to perform a detailed study of the physical properties of Heusler alloys Ni_2MnSb and NiMnSb and their continuous series $Ni_{2-x}MnSb$. Finite-temperature studies of spin fluctuations and corresponding Curie temperatures are obtained from the multisublattice Heisenberg Hamiltonian derived from corresponding first-principles calculations. The Heisenberg Hamiltonian was constructed by a direct evaluation of exchange parameters in real space using an approach described in detail in Refs. 2 and 4 and generalized to the case of complex lattices and disordered systems.[9] In addition to the MFA, we have also employed the multisublattice random-phase approximation[16] (RPA) and Monte Carlo simulation[8] (MCS) methods to estimate the corresponding critical temperatures of the Heisenberg Hamiltonian. We will also study the variation of the Curie temperature under the external pressure, evaluate the magnon spectra, and investigate magnetic short-range order in the paramagnetic state above the Curie temperature for both alloys.

Because exchange interactions and related critical temperatures can depend on the details of the mapping procedure, we have also investigated their dependence on electron correlations, the reference state used for mapping and its possible versions, and the effect of electronic entropy with the aim to establish the theoretical "error bar" of the present approach.

II. METHOD OF CALCULATION

In this section we briefly summarize the calculational approaches used to determine the electronic structure, exchange integrals, and Curie temperatures of $Ni_{2-x}MnSb$ alloys.

A. Electronic structure

Electronic structure calculations were performed within the tight-binding linear muffin-tin orbital (TB-LMTO) method and the atomic sphere approximation (ASA) using the *spd* basis set. The effect of disorder was described by the coherent-potential approximation (CPA) as implemented in the framework of the TB-LMTO method.[17] We employ as a reference state for the construction of the Heisenberg Hamiltonian both the ferromagnetic (FM) and the disordered local moment (DLM) states (see also Ref. 10). The DLM state can be naturally treated in the framework of the CPA: the Mn moments have collinear but random positive (Mn^+) and negative (Mn^-) orientations and similarly for Ni moments.[17] For example, the NiMnSb ordered alloy is treated as a multicomponent random alloy $(Ni^+_{0.5}Ni^-_{0.5}Mn^+_{0.5}Mn^-_{0.5})Sb$ and similarly for other alloys. Empty spheres were introduced for NiMnSb at the place of missing fcc sublattice for a good space filling. This sublattice is partially (fully) occupied by Ni atoms in the case of $Ni_{2-x}MnSb$ (Ni_2MnSb) alloys. Lattice parameters were taken from the experiment.[18]

B. Calculation of exchange parameters

The classical multisublattice Heisenberg Hamiltonian in the zero external magnetic field can be written in the following form:

$$H = -\sum_{ij,\alpha\beta} J_{ij}^{\alpha\beta} \mathbf{e}_i^{\alpha} \cdot \mathbf{e}_j^{\beta}, \tag{1}$$

where $J_{ij}^{\alpha\beta}$ are exchange parameters, i,j are unit cell indices, α,β are sublattice indices, and $\mathbf{e}_i^{\alpha}$ is the unit vector parallel to the magnetization at the site i on the sublattice α. The positive (negative) values of $J_{ij}^{\alpha\beta}$ correspond to the ferromagnetic (antiferromagnetic) couplings, respectively, and the magnitudes of corresponding magnetic moments are included in the definition of $J_{ij}^{\alpha\beta}$. In random alloys, an additional index labeling an atom type Q on a given sublattice will appear—e.g., $Q=A$, B for a binary alloy of elements A and B. As will be obvious later, in the present case we can still keep the above simpler notation even for the case of $Ni_{2-x}MnSb$ alloys. The translational symmetry of the crystal (or of the configurationally averaged random alloy) implies $J_{ij}^{\alpha\beta}=J_{i-j,0}^{\alpha\beta}$ while the on-site terms are zero: namely, $J_{ii}^{\alpha\alpha}=0$.

The exchange interactions were obtained by mapping *ab initio* electronic structure calculations to the classical Heisenberg Hamiltonian.[2] In the the framework of the TB-LMTO-ASA method we obtain[4,9]

$$J_{ij}^{\alpha\beta} = \frac{1}{8\pi i} \int_C \mathrm{tr}[\Delta_i^{\alpha}(z) g_{ij}^{\alpha\beta,\uparrow}(z) \Delta_j^{\beta}(z) g_{ji}^{\beta\alpha,\downarrow}(z)] dz. \tag{2}$$

The energy integration is performed along a contour in the complex plane which encircles occupied part of valence band and the trace runs over the angular momentum indices $L=(\ell,m)$. The quantities $g_{ij}^{\alpha\beta,\sigma}(z)$ $(\sigma=\uparrow,\downarrow)$ and $\Delta_i^{\alpha}(z)$ are, respectively, the site off-diagonal blocks of the auxiliary Green functions and differences $P_{i\uparrow}^{\alpha}(z)-P_{i\downarrow}^{\alpha}(z)$ of the potential functions $P_{i\sigma}^{\alpha}(z)$ of the TB-LMTO-ASA method.[17] For the dominating d states are $\Delta_i^{\alpha}(z)$ proportional to the corresponding exchange splitings (local magnetic moments) on atoms.[11] A similar expression can be also used to derive exchange parameters in random alloys: the auxiliary Green function is then substituted by its conditionally averaged counterpart evaluated in the framework of the CPA.[9] In the case of the DLM state one has to take into account in addition the sign change for Mn^- sites: all corresponding interactions among $Mn^{\pm}$ sites are then the same. It should be noted that exchange interactions estimated from the DLM reference states are in general more localized because of damping introduced by the spin-disorder treated in the framework of the CPA.

C. Calculation of transition temperatures

We will determine the Curie temperature T_C in the framework of the MFA, RPA, and MCS approaches. The Curie temperature in the framework of the multisublattice MFA Refs. 5, 11, and 16 is related to an eigenvalue problem of the real symmetric matrix $\mathbb{J}(\mathbf{0})$ with elements $J^{\alpha\beta}(\mathbf{0})$: namely,

$$\sum_{\beta} J^{\alpha\beta}(\mathbf{0}) \langle e_z^{\beta} \rangle = \frac{3k_B T_C}{2} \langle e_z^{\alpha} \rangle,$$

$$J^{\alpha\beta}(\mathbf{0}) = \sum_i J_{0i}^{\alpha\beta}, \tag{3}$$

where $\langle e_z^{\alpha} \rangle$ is the thermodynamically averaged z component of the unit vector $\mathbf{e}_i^{\alpha}$ and k_B is the Boltzmann constant. The MFA critical temperature T_C^{MFA} is then given by the maximum eigenvalue of the $\mathbb{J}(\mathbf{0})$ matrix.[5,11,19]

The evaluation of the Curie temperature within the RPA for more than one sublattice requires an iterative calculation. The averages $\langle e_z^{\alpha} \rangle$ are connected with the lattice Fourier transform of exchange interactions, $J^{\alpha\beta}(\mathbf{q})=\Sigma_i J_{0i}^{\alpha\beta} e^{i\mathbf{q}\cdot\mathbf{R}_{0i}}$, by the following expression:[16]

$$\langle e_z^{\alpha} \rangle = \frac{2}{3k_B T_C^{RPA}} \left(\frac{1}{\Omega} \int d\mathbf{q} [\mathbb{N}^{-1}(\mathbf{q})]^{\alpha\alpha} \right)^{-1}, \tag{4}$$

where T_C^{RPA} is the RPA estimate of the Curie temperature, Ω is a volume of the first Brillouin zone, and the elements $N^{\alpha\beta}(\mathbf{q})$ of the matrix $\mathbb{N}(\mathbf{q})$ are given by

$$N^{\alpha\beta}(\mathbf{q}) = \delta_{\alpha\beta} \sum_{\gamma} J^{\alpha\gamma}(\mathbf{0}) \langle e_z^{\gamma} \rangle - \langle e_z^{\alpha} \rangle J^{\alpha\beta}(\mathbf{q}). \tag{5}$$

In the case of a simple lattice this result reduces to that in Ref. 4. The zero step $\langle e_z^{\alpha} \rangle$ can be obtained from the mean-field sublattice values and then we iterate Eqs. (4) and (5) until self-consistency is achieved. The RPA Curie temperature is always lower than the corresponding MFA value, $T_C^{RPA} < T_C^{MFA}$.[16] In the case that all $J_{ij}^{\alpha\beta}$ are positive (ferromagnetic), it can be shown that T_C^{RPA} represents a lower estimate

of the critical temperature.[20] On the other hand, the MFA neglects spin fluctuations and therefore magnetic moments are artificially more rigid and critical temperatures overestimated.[19]

Alternatively, Eq. (4) can be considered as a limit $T \rightarrow T_C$ of a more general expression

$$\langle e_z^\alpha \rangle = \mathcal{L}\left[\frac{2}{k_B T}\left(\frac{1}{\Omega}\int d\mathbf{q}[\mathbb{N}^{-1}(\mathbf{q})]^{\alpha\alpha}\right)^{-1}\right], \tag{6}$$

where $\mathcal{L}(x)=\coth(x)-1/x$ is the Langevin function. This allows us to calculate the magnetization as a function of the temperature. The temperature T at which $\langle e_z^\alpha \rangle$ (T) goes to zero coincides with T_C as obtained by Eq. (4). The determination of T_C from Eq. (6) is much more demanding computationally, but on the other hand, it is more robust and provides more complete information about the system. For more details concerning the multisublattice RPA we refer to our recent paper.[16]

We have two remarks concerning the numerical evaluation of T_C in the RPA. The divergence occurring in the integrand at $\mathbf{q}=0$ [see Eq. (4)] is treated here by an analytic deconvolution method[4] which employs the relation $f(0) \approx 4f(i\varepsilon)-f(2i\varepsilon)-f(\varepsilon+i\varepsilon)-f(-\varepsilon+i\varepsilon)$ valid for any analytical function and exact up to the fourth order in ε. The deconvolution parameter ε is a small real number as compared to $k_B T_C$. The resulting T_C is slightly increased proportionally to ε, and the estimated error is of order of few K. We have verified that the neglect of small induced magnetic moments on the Sb sublattice (eventually on the sublattice of empty spheres in NiMnSb and $Ni_{2-x}MnSb$) has led to a negligible error of about ±1 K. This fact has been used in the numerically demanding MCS studies while all sublattices were included in the case of the RPA.

We have also investigated the dependence of T_C on the cutoff parameter R_{max} of exchange interactions. While T_C^{RPA} is nearly converged already for $R_{max} \approx 2a$ in the NiMnSb alloy due to the exponential damping of interactions with a distance (see Sec. III B), T_C^{RPA} for the Ni_2MnSb compound with long-range interactions does not converge even for $R_{max}=4a$. To overcome this difficulty, we have employed an approach similar to that used in Ref. 4. We replace $J_{ij}^{\alpha\beta}$ by $J_{ij}^{\alpha\beta}\exp(-\eta R_{ij}^{\alpha\beta})$, where $R_{ij}^{\alpha\beta}$ denotes the distance between the $i\alpha$ and $j\beta$ sites, and calculate T_C as a function of the damping parameter $\eta > 0$—i.e., $T_C=T_C(\eta)$. For a large enough η the $T_C(\eta)$ converges quickly with R_{max} and the Curie temperature is obtained by extrapolating $T_C(\eta)$ to $T_C(\eta=0)$. The extrapolated values using linear and parabolic fits were almost the same, and the estimated error was less than 10 K in the least favorable case of the ordered Ni_2MnSb alloy with long-range interactions.

The MCS has employed the Metropolis algorithm where the critical temperature was evaluated by means of the cumulant crossing method.[21] In this method, it has been shown that the fourth-order cumulant $U_4=1-\langle (e_z^\alpha)^4\rangle / 3\langle (e_z^\alpha)^2\rangle^2$ has a size-independent universal fixed point U^* at $k_B T_c$. In this way, T_c is extracted from the unique intersection point U^* when U_4 is calculated for a number of different lattice sizes as a function of temperature. We have therefore calculated U_4 for a number of different lattice sizes on the Mn and Ni sublattices and the total number of sites was varied between 4096 and 32 768 for NiMnSb and between 6144 and 49 152 for Ni_2MnSb. The thermal average of the magnetization was measured for around 50 000 Monte Carlo steps per lattice site.

The MCS is demanding computationally and therefore one has to limit the number of exchange interactions taken into consideration (the cutoff parameter R_{max}), in particular for the case of a few sublattices. Numerous tests have shown that the sensitivity of the MCS to the cutoff parameter R_{max} is roughly similar to that of the MFA. This makes it possible to restrict R_{max} used in simulations to the value where the MFA sum (3) converges. The long-range behavior of exchange interactions found in Ni_2MnSb makes evaluation of the Curie temperature more difficult as compared to the NiMnSb case because a larger number of shells has to be used to obtain well-converged results. The neglect of $J_{ij}^{\mathrm{Mn,Ni}}$ and $J_{ij}^{\mathrm{Ni,Ni}}$ interactions influences the resulting Curie temperatures only weakly (see Sec. III A). Using this fact, we used the MCS, employing only Mn-Mn interactions, but with the cutoff set to $R_{max}=3.24a$. Only for NiMnSb with well-localized exchange interactions did we also do calculations including both $J_{ij}^{\mathrm{Mn,Ni}}$ and $J_{ij}^{\mathrm{Ni,Ni}}$ but with a smaller cutoff of $R_{max}=2.236a$. Unfortunately, we were unable to estimate the error bar of these choices because the numerical effort to get such estimates is too large.

The evalution of Curie temperatures of random $Ni_{2-x}MnSb$ alloys is facilitated by the fact that the Mn sublattice, one of the Ni sublattices, and the Sb sublattice are nonrandom. The evaluation of the Curie temperature is thus straightforward for a model which employs only $J^{\mathrm{Mn,Mn}}$ interactions: the calulations proceed like in an ordered case but with $J^{\mathrm{Mn,Mn}}$ and $J^{\mathrm{Mn,Ni}}$ interactions between spins on nonrandom Mn and Ni sublattices modified by the alloy disorder. The multisublattice calculations will be done in the framework of the average lattice model for random interactions[9] $\tilde{J}^{\mathrm{Mn,Ni}}$ between Mn spins and Ni spins on the partially filled Ni sublattice. In this approximation we substitute the disordered lattice by an ordered one with effective interactions—namely, $\tilde{J}_{\mathrm{eff}}^{\mathrm{Mn,Ni}}=x\tilde{J}^{\mathrm{Mn,Ni}}$, where x is the concentration of Ni atoms on the disordered sublattice—and we neglect the contribution from empty sites. The average lattice approximation is inapplicable for diluted systems with localized interactions due to the effect of magnetic percolation.[8] Here, even for the lowest Ni concentration ($Ni_{1.25}MnSb$) we are beyond the percolation limit for the fcc lattice. In addition, the exchange interactions $\tilde{J}^{\mathrm{Mn,Ni}}$ are very small (see Sec. III B), thus further reducing a possible error introduced by the average lattice approximation. Random alloys were studied only using the MFA and RPA approaches.

Finally, it should be mentioned that the present construction of the Heisenberg Hamiltonian on which estimates of the Curie temperature are based is exact in the long-wave limit—i.e., for $\mathbf{q} \rightarrow 0$.[15,22] It is thus particularly suitable for the RPA calculations, results of which depend strongly on a correct description of $J(\mathbf{q})$ for $\mathbf{q}$ close to zero. It is possible to go beyond this limit by using the "exact" approach based on linear response theory.[15] We shall employ here an equiva-

lent renormalized magnetic force theorem formulation of Bruno.[22] This formulation is particularly simple for the RPA in the limit neglecting Mn-Ni interactions: the corresponding correction enhances T_C according to the expression[22] (the renormalized RPA)

$$\tilde{T}_C^{RPA} = T_C^{RPA}\left(1 - 6\frac{k_B T_C^{RPA}}{m^{\mathrm{Mn}}\delta^{\mathrm{Mn}}}\right)^{-1}. \quad (7)$$

Here, m^{Mn} denotes the average magnetic moment (in μ_B) on the Mn sublattice and δ^{Mn} denotes the corresponding averaged exchange splitting on Mn atoms estimated from the present LSDA calculations.

III. RESULTS AND DISCUSSION

A. Electronic structure

NiMnSb and Ni_2MnSb ordered alloys crystallize in $C1_b$ and $L2_1$ structures, respectively.[18] Two structural models are thus possible for $Ni_{2-x}MnSb$ alloys: namely, $C1_b$- and $L2_1$-like structures. In the former one, the Ni atoms gradually occupy interstitial sites in the ordered NiMnSb in an amount $1-x$ while in the latter case there is a symmetric occupation of both Ni sublattices in the ordered Ni_2MnSb alloy by vacancies in an amount $x/2$ each. The *ab initio* calculations, either simulating disordered alloys by ordered supercells[13] or based on the description of the disorder in the framework of the CPA as in the present case, agree on the energetical preference of the $C1_b$ structure. X-ray and neutron diffraction experiments confirm this result for $x \geqslant 0.3$ while a more complex picture emerges for $x < 0.3$ with a possible chemical disorder among Mn, Ni, and vacant sites.[18] The details of possible arrangements are not known, and we will assume the $C1_b$ structure for all studied random alloys: $Ni_{1.25}MnSb$, $Ni_{1.5}MnSb$, and $Ni_{1.75}MnSb$.

The densities of states (DOS) for NiMnSb, $Ni_{1.5}MnSb$, and Ni_2MnSb alloys are presented in Fig. 1. Two competing effects influence the bandwidth of NiMnSb as compared to Ni_2MnSb: the slightly smaller (about 1.3%) lattice constant and smaller coordination of Mn atoms with Ni neighbors. The net effect is a narrower *d*-band width in NiMnSb as seen in Fig. 1; i.e., the smaller coordination prevails.

However, the most remarkable difference between NiMnSb and Ni_2MnSb is the half-metallicity of NiMnSb: the Fermi energy lies in the gap of the minority states. This fact has a pronounced influence on the behavior of exchange parameters as a function of the distance (see Sec. III B) because exchange parameters depend sensitively on the electronic states at the Fermi energy and the Fermi surface topology in particular. It is thus obvious from Fig. 1 that the behavior of exchange parameters will be dominated by minority electrons. The partial occupation of interstitial sites in random $Ni_{2-x}MnSb$, $x=0.25$, 0.5, and 0.75, adds electrons to the valence band and destroys the half-metallicity and all alloys are metals, similarly as Ni_2MnSb. This is illustrated in Fig. 1 for $Ni_{1.5}MnSb$ alloy. The critical concentration of Ni atoms on the interstitial sublattice for the disappearance of the gap in minority states we found at approximately 12%.

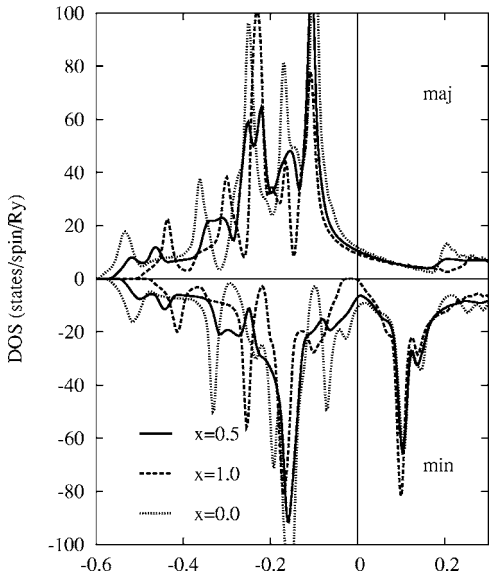

FIG. 1. Total densities of states for $Ni_{2-x}MnSb$ alloys resolved with respect to the spin: ordered NiMnSb ($x=1$) and Ni_2MnSb ($x=0$) alloys and the disordered $Ni_{1.5}MnSb$ ($x=0.5$) alloy. The alloy Fermi energies are shifted to the zero of energy.

The calculated local magnetic moments of $Ni_{2-x}MnSb$ alloys for ambient pressure and under pressure are summarized in Table I. Calculated values depend weakly on the alloy composition and are in a fair agreement with available experimental values[18] as well as with recent theoretical calculations.[5,11,12] The local moments on Mn sites dominate

TABLE I. Calculated unit cell and local magnetic moments on given atoms for $Ni_{2-x}MnSb$ alloys in μ_B. The experimental unit cell moments are, respectively, $(4.0\pm0.3)\mu_B$ (Ref. 18). For alloys ($0<x<1$) two Ni sublattices (filled and partially filled) have different local magnetic moments. The local Ni moments on the partially filled sublattices are shown in brackets. Values in parentheses correspond to the local moments for ordered alloys under pressure (the reduction of experimental lattice constant by 3%).

	Unit cell	Local Mn	Local Ni	Local Sb
NiMnSb	4.00 (3.94)	3.77 (3.63)	0.226 (0.274)	−0.062 (−0.038)
$Ni_{1.25}MnSb$	3.91	3.73	0.196 [0.019]	−0.060
$Ni_{1.5}MnSb$	3.84	3.68	0.168 [0.035]	−0.055
$Ni_{1.75}MnSb$	3.78	3.62	0.143 [0.071]	−0.043
Ni_2MnSb	3.70 (3.52)	3.52 (3.31)	0.105 (0.118)	−0.032 (−0.026)

TABLE II. Critical temperatures (in kelvin) of $Ni_{2-x}MnSb$ alloys for various approximations. The symbols MFA, RPA, r-RPA, and MCS label the mean-field approximation, the random-phase approximation, the renormalized random-phase approximation [Eq. (7)], and the Monte Carlo simulation results, respectively. Experimental values (Expt.) are from Ref. 18. The ferromagnetic reference state was used in the mapping. Critical temperatures are estimated using exchange interactions on all sublattices (all subl) eventually on Mn and Ni sublattices for the MCS and on the Mn sublattice (Mn-Mn) only. Results for calculated critical temperatures of ordered NiMnSb and Ni_2MnSb alloys under pressure corresponding to a 3% reduction of the lattice constant are also presented (symbol $*$). For NiMnSb and Ni_2MnSb alloys we include also results obtained for the reference DLM state. In this case, only exchange interactions between Mn moments are nonzero.

	$Ni_{2-x}MnSb$ alloys				
	MFA	RPA	r-RPA	MCS	Expt.
NiMnSb (all subl)	1106	880		940	732
NiMnSb (Mn-Mn)	1069	852	881	910	
NiMnSb (DLM, Mn-Mn)	1536	1132	1185	1210	
$Ni_{1.25}MnSb$ (all subl)	910	697			570
$Ni_{1.25}MnSb$ (Mn-Mn)	884	678	696		
$Ni_{1.5}MnSb$ (all subl)	739	523			456
$Ni_{1.5}MnSb$ (Mn-Mn)	723	510	521		
$Ni_{1.75}MnSb$ (all subl)	609	408			405
$Ni_{1.75}MnSb$ (Mn-Mn)	600	401	408		
Ni_2MnSb (all subl)	575	360			368
Ni_2MnSb (Mn-Mn)	570	356	356	380	
Ni_2MnSb (DLM, Mn-Mn)	662	348	353	380	
$NiMnSb^*$ (all subl)	1085	875			Not available
Ni_2MnSb^* (all subl)	655	450			>400

the total moment per unit cell, but we find also small induced moments on Ni and Sb sites, the latter with opposite sign (see also Refs. 5 and 11). Even smaller induced local moments are found for Ni sites on partially filled disordered Ni sublattices, in good quantitative agreement with supercell calculations in Ref. 13. Within the DLM approach the local Mn moments for NiMnSb and Ni_2MnSb are, respectively, $3.76\mu_B$ and $3.43\mu_B$, while the Ni and Sb local moments have collapsed to zero. The weak dependence on the reference state (the FM and DLM states) is related to the large local Mn moments, and it also justifies the use of the adiabatic approximation for the evaluation of exchange parameters.[4,15]

The calculations under pressure were done for the lattice constant reduced about 3% as compared to the experimental one which roughly correspond to the experiment done on Ni_2MnSb.[23] No experimental data are available for NiMnSb, and we have therefore assumed the same reduction of the lattice constant as for Ni_2MnSb. We observe the decrease of local Mn moments which is due to the increasing overlap of wave functions resulting from reduced interatomic distances. On the other hand, Ni moments increased due to stronger hybridization. Similar results were obtained recently in an extensive study of the physical properties of Ni_2MnSb under pressure.[12] The unit cell moment for NiMnSb under pressure is smaller than $4\mu_B$, indicating that the alloy is no longer a half-metal. This will have a pronounced effect on exchange interactions [see Fig. 3(b)].

Total energy calculations confirm the stability of the FM state as compared to the DLM state: $E_{\mathrm{DLM}}-E_{\mathrm{FM}}=15.09$ mRy and 6.43 mRy per formula unit for NiMnSb and Ni_2MnSb, respectively. Consequently, one can expect that the Curie temperature of NiMnSb will be more than 2 times larger as compared to Ni_2MnSb (see Table II).

B. Exchange interactions

The calculated exchange interactions between Mn-Mn and Mn-Ni pairs in NiMnSb, $Ni_{1.5}MnSb$, and Ni_2MnSb alloys are shown in Fig. 2. Exchange interactions are in general reduced with increasing Ni content, but their detailed behavior as a function of Ni concentration is rather complex. With increasing Ni content the leading first nearest-neighbor (NN) interactions on the Mn sublattice, $J_1^{\mathrm{Mn,Mn}}$, are reduced less as compared to the second NN but the fourth NN interactions at the same time increase. Such irregular behavior indicates the crossover from the RKKY-type behavior of exchange interactions in metallic Ni_2MnSb with a pronounced oscillatory behavior to the exponentially damped and more localized interactions in the half-metallic NiMnSb (see below). In random $Ni_{2-x}MnSb$ alloys there are two kinds of

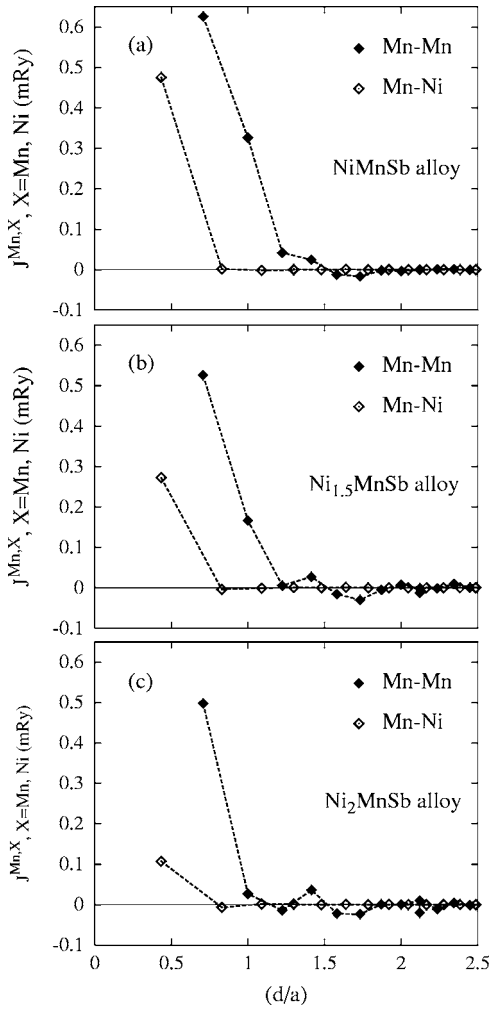

FIG. 2. Exchange interactions $J^{\mathrm{Mn,Mn}}$ and $J^{\mathrm{Mn,Ni}}$ as a function of the interatomic distance d (in units of the lattice constant a): (a) the ordered half-metallic NiMnSb, (b) the metallic disordered $Ni_{1.5}MnSb$ alloys, and (c) the ordered metallic Ni_2MnSb.

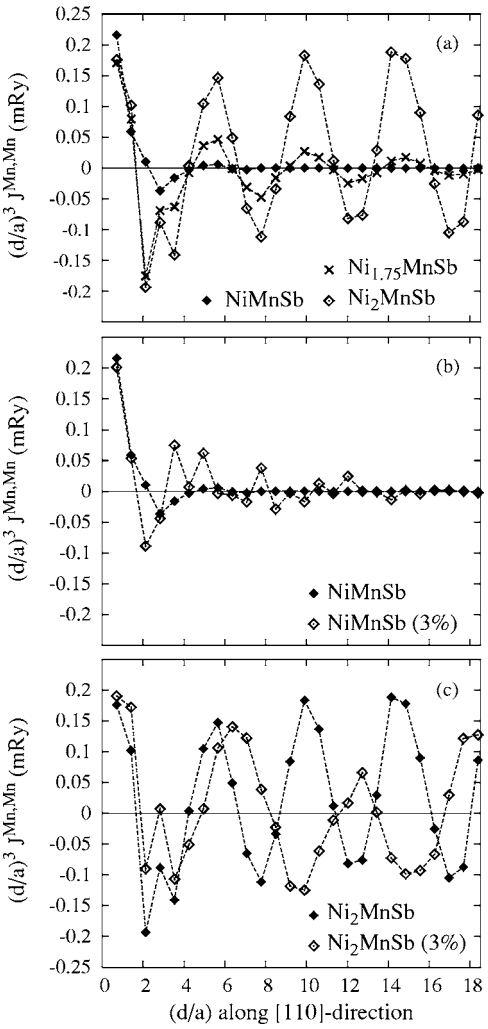

FIG. 3. Exchange interactions $J^{\mathrm{Mn,Mn}}$ along the direction [110] on the Mn sublattice: (a) $Ni_{2-x}MnSb$ for $x=0$, 0.25, and 1.0, (b) NiMnSb at ambient pressure and at the presure corresponding to the lattice constant reduced by 3%, and (c) the same as in (b) but for Ni_2MnSb.

exchange interactions between Mn and Ni sites—namely, $J^{\mathrm{Mn,Ni}}$ and $\tilde{J}^{\mathrm{Mn,Ni}}$—which characterize, respectively, the interactions of Mn spins with Ni spins on the fully occupied and partially occupied (random) Ni sublattices.

$J^{\mathrm{Mn,Ni}}$ exchange interactions are strongly localized, ferromagnetic in all compounds, and their absolute values decrease strongly from NiMnSb to Ni_2MnSb—i.e., with increasing Ni content. The reason can be seen from Eq. (2): assuming a rigid band model,[11] $J^{\mathrm{Mn,Ni}}$ are proportional to the factor $m^{\mathrm{Mn}}m^{\mathrm{Ni}}$; i.e., they are reduced in Ni_2MnSb 2.3 times as compared to NiMnSb (see Table I). Despite the fact that in NiMnSb and $Ni_{1.5}MnSb$ alloys $J_1^{\mathrm{Mn,Ni}}$ and $J_1^{\mathrm{Mn,Mn}}$ are comparable in size, the effect of $J^{\mathrm{Mn,Ni}}$ exchange interactions on the Curie temperature is weak (see Table II), in particular for Ni_2MnSb. The reason is their localized character (only $J_1^{\mathrm{Mn,Ni}}$ are relevant) and the small coordination (4NN) in which they appear, e.g., in the MFA sum [Eq. (3)]. On the contrary, many $J^{\mathrm{Mn,Mn}}$ contribute to the MFA sum with large weights (e.g., there are 12 $J_1^{\mathrm{Mn,Mn}}$ NN). $\tilde{J}^{\mathrm{Mn,Ni}}$ exchange interactions (not shown in Fig. 2) are also strongly localized and ferromagnetic, and their values decrease monotonically with increasing x in $Ni_{2-x}MnSb$ alloys. For example, the dominating $\tilde{J}_1^{\mathrm{Mn,Ni}}$ in $Ni_{1.5}MnSb$ is about 5 times smaller as compared to $J_1^{\mathrm{Mn,Ni}}$ in Ni_2MnSb. Consequently, their effect, e.g., on the Curie temperature will be even weaker as is the effect of $J^{\mathrm{Mn,Ni}}$ discussed above.

The behavior of exchange interactions $J^{\mathrm{Mn,Mn}}$ as a function of the interatomic distance d_{ij} is illustrated in Fig. 3 along the dominating [110] direction. It should be noted that exchange interactions $J^{\mathrm{Mn,Mn}}(d_{ij})$ are now multiplied by a factor d_{ij}^3 typical for the Ruderman-Kittel-Kasuya-Yosida (RKKY) interaction. We observe well-pronounced long-range oscillatory behavior in Ni_2MnSb mediated by *sp* electrons at the Fermi energy (see Fig. 1) with exchange interactions decreasing with the distance d as d^{-3} [Fig. 3(a)]. Exchange interactions $J^{\mathrm{Mn,Mn}}$ in Ni_2MnSb thus exhibit RKKY-like behavior similar to that found for Fe impurities in AuFe alloy with a free-electron-like Au host.[24] Here, however, the magnetic atoms occupy each site of the Mn sublattice as contrasted to randomly distributed Fe impurities

found in diluted canonical spin-glass alloys. It should be noted that we also observe a preasymptotic region for small interatomic distances as well as a strong space anisotropy of interactions along different directions (not shown) found recently also for the diluted magnetic semiconductors.[9] Such an anisotropy is clearly related to the space anisotropy of the underlying lattice as contrasted to the isotropic dependence found in the free-electron host (the conventional RKKY model).

The behavior of exchange interactions in the half-metallic NiMnSb is strikingly different. The Fermi energy in the gap of minority states (see Fig. 1) leads to an exponential damping of the corresponding Green function $g_{ij}^{\beta\alpha,\downarrow}(z)$ with distance d_{ij}, and the same is also true for exchange interactions, Eq. (2), as explained in detail in Refs. 4 and 9.

The effect of disorder in the incompletely occupied Ni sublattice is illustrated for $Ni_{1.75}MnSb$ alloy. The dominating feature is the onset of oscillations due to the crossover from the half-metallic behavior in NiMnSb to the metallic one in $Ni_{1.75}MnSb$. There is a strong disorder between d states on Ni atoms and vacant sites (the split-band regime[17]) but the states on the nonrandom Mn sublattice at the Fermi energy are influenced by this disorder only indirectly, via the hybridization. Nevertheless, this disorder leads to a small damping of RKKY-like oscillations with distance as contrasted with case of the ordered Ni_2MnSb alloy.

In the same way, an observed onset of oscillations in NiMnSb under pressure, Fig. 3(b), is a precursor of its metallic state. The applied pressure modifies electronic states and hence also the Fermi surface topology of Ni_2MnSb and, consequently, leads to modified periods and amplitudes of oscillations as illustrated in Fig. 3(c).

A simple application of calculated exchange parameters is the evaluation of the spin-wave spectra $E(\mathbf{q})$ corresponding to the Mn-Mn interactions,[5] which is given by the expression[4]

$$E(\mathbf{q}) = \frac{4}{m^{\mathrm{Mn}}}[J^{\mathrm{Mn,Mn}}(\mathbf{0}) - J^{\mathrm{Mn,Mn}}(\mathbf{q})]. \tag{8}$$

Here, m^{Mn} is the local magnetic moment (in μ_B) on the Mn sublattice (see Table I) and $J^{\mathrm{Mn,Mn}}(\mathbf{q})$ is the lattice Fourier transform of the real space $J_{ij}^{\mathrm{Mn,Mn}}$, Eq. (2). The calculated spin-wave spectra are presented in Fig. 4 along the lines of high symmetry in the first Brillouin zone. The results for Ni_2MnSb alloy along the line Γ-X agree well with those calculated using the frozen-magnon approach.[5] The negative slopes in the magnon spectra of Ni_2MnSb are known as Kohn anomalies. Such anomalies were found earlier, e.g., in the spin-wave spectra of the ferromagnetic bcc Fe crystal.[4,25] It should be noted that a large number (of order 100) of $J^{\mathrm{Mn,Mn}}$ exchange interactions is needed to recover them from the lattice Fourier transform of real-space exchange interactions.[4] The experimental finding of Kohn anomalies is difficult due to the finite lifetime of magnons close to the zone boundaries and due to a possible merging of spin-wave spectra into the continuum of Stoner excitations. The spin-wave spectrum of NiMnSb exhibits larger curvature at $\mathbf{q}=\mathbf{0}$,

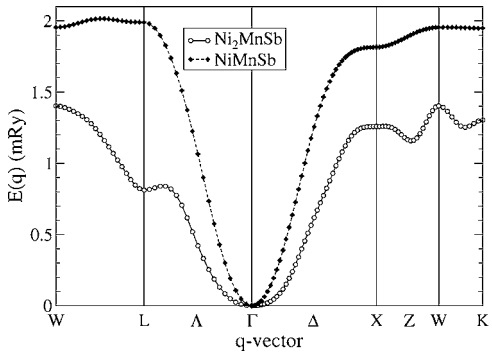

FIG. 4. Spin-wave spectra of Mn atoms in NiMnSb and Ni_2MnSb alloys evaluated along the lines of high symmetry of the fcc Brillouin zone.

thus indicating a larger spin-wave stiffness constant of NiMnSb as compared to Ni_2MnSb.

C. Curie temperatures

The calculated Curie temperatures for $Ni_{2-x}MnSb$ alloys (see Table II) decrease with the increasing Ni concentration, in agreement with the experiment.[18] We also reproduce the faster decrease of the Curie temperature from NiMnSb to $Ni_{1.5}MnSb$ as compared to its decrease from $Ni_{1.5}MnSb$ to Ni_2MnSb. The experimental Curie temperatures over the whole concentration range are also in fair quantitative agreement with the RPA estimates, the agreement being better for Ni-rich alloys. The MCS values (when available) are slightly higher as compared to the RPA ones but both the RPA and MCS estimates compare with the experiment much better as compared to the MFA values.

In Table II we also present estimates of the Curie temperature of ordered NiMnSb and Ni_2MnSb under pressure. In agreement with the experiment[23] as well as with the study employing the frozen-magnon approach[12] we obtain an increase of the Curie temperature of Ni_2MnSb with pressure. On the contrary, the change of the Curie temperature with pressure is very weak for the half-metallic NiMnSb alloy. We present in Fig. 5(a) the pressure dependence of exchange interactions in Ni_2MnSb which explain an increase of the Curie temperature with pressure.

D. Spin-spin correlation function

It is also interesting to study the character of spin fluctuations above the Curie temperature in the paramagnetic region. We have evaluated the real-space spin-spin correlation function

$$G(\mathbf{r}_{ij}) = G(\mathbf{r}_i - \mathbf{r}_j) = \langle \mathbf{e}_i \cdot \mathbf{e}_j \rangle \tag{9}$$

by using the Monte Carlo method similarly to the case of ferromagnetic transition metals.[28] Here, $G(\mathbf{0})=1$, and $G(\mathbf{r}_{ij})$ is an overall decreasing function with respect to the distance. The system lacks long-range order if $G(\mathbf{r}_{ij})$ goes to zero at long distances. The inverse correlation length κ, which can be measured experimentally, can be estimated by fitting the calculated $G(\mathbf{r}_{ij})$ as a function of the distance $d=|\mathbf{r}_{ij}|$ to the

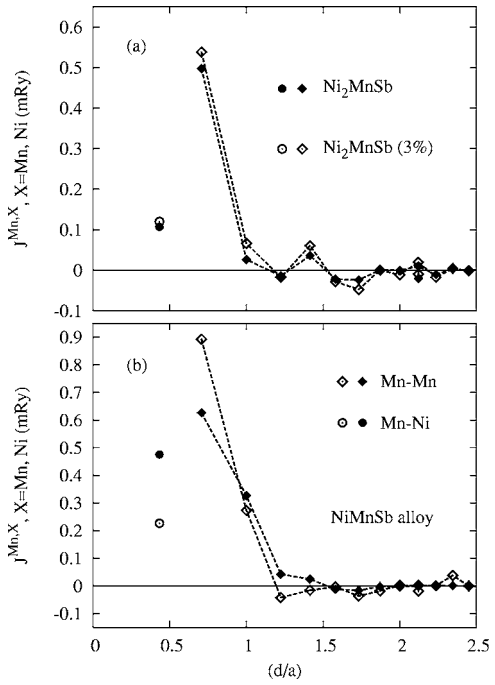

FIG. 5. Exchange interactions $J^{\mathrm{Mn,Mn}}$ (diamonds) and $J^{\mathrm{Mn,Ni}}$ (circles) as a function of the interatomic distance d (in units of the lattice constant a): (a) the metallic Ni_2MnSb alloy at the ambient pressure (full symbols) and at the pressure corresponding to 3% reduction of the lattice constant (empty symbols), and (b) the half-metallic NiMnSb at the LSDA (full symbols) and LSDA+U (empty symbols). In both cases only dominating $J_1^{\mathrm{Mn,Ni}}$ are shown.

Ornstein-Zernicke form $G(d) \propto \exp(-\kappa d)/d$. A related quantity, which characterizes the amount of magnetic short-range order in the system, is the averaged angle between the nearest-neighbor spins, α_{NN}. In a fully correlated ferromagnetic state it is $\alpha_{NN}=0°$ while for random spins without correlation is $\alpha_{NN}=90°$. In Fig. 6 we show the spin-spin correlation function calculated as a function of the distance between spins for two temperatures in the paramagnetic state just above the corresponding Curie temperature. A fit to the Ornstein-Zernicke form, valid in the long-wavelength limit, was done by omitting the first two nearest neighbors. Similarly to the case of bcc Fe,[28] we observe only small deviations of $G(d)$ as a function of d from the monotonically decreasing Ornstein-Zernicke form. The results depend very weakly on the choice of reference state used for mapping: namely, the fully correlated FM state and disordered DLM state. The higher values of the correaltion functions in Ni_2MnSb as compared to NiMnSb reflect the more localized exchange interactions in the latter system. The calculated α_{NN} for NiMnSb (Ni_2MnSb) at T_c is 79° (69°) which should be compared with $\alpha_{NN}=74°$ for bcc Fe.[28] These values slightly increase with temperature. There is thus a relatively small amount of magnetic short-range order in the paramagnetic region in both alloys. Finally, the inverse correlation lengths κ expressed in units of the inverse lattice constant are 1.200 (0.986) for NiMnSb (Ni_2MnSb) at $T \approx 1.2T_c$. These values compare well with bcc Fe for which $\kappa=1.05$ for $T=1.25T_c$. We did not find corresponding experimental values for Heusler alloys.

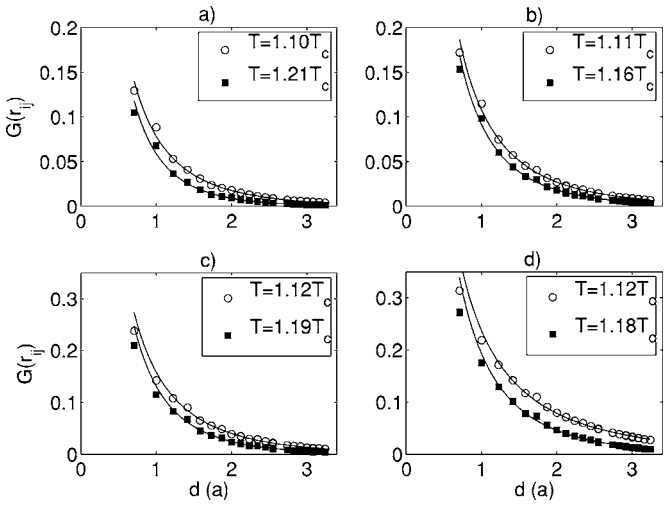

FIG. 6. Dependence of the real-space spin-spin correlation function $G(\mathbf{r}_{ij})$ on the distance $\mathbf{r}_{ij}$ (in units of lattice constant a) for two temperatures above the corresponding Curie temperatures and for the ferromagnetic (FM) and disordered local moment (DLM) reference states: (a) NiMnSb, FM; (b) NiMnSb, DLM; (c) Ni_2MnSb, FM; and (d) Ni_2MnSb, DLM.

E. Curie temperature and computational parameters

Most of calculations in this paper were done by using the LSDA, the FM reference state, and the mapping assuming the adiabatic approximation. This is a conventional approach also employed in related papers[5,11–13] in the field. A noticeable exception is a recent study of the bcc Fe (Ref. 10) in which the DLM reference state was used. We wish therefore to discuss the robustness of the calculated Curie temperatures with respect to some factors which can influence it. In particular, we consider the effect of (i) electron correlations beyond the LSDA, (ii) the choice of the reference state for mapping, (iii) the mapping itself, and (iv) the influence of the electronic entropy.

The effect of electron correlations on the electronic structure of NiMnSb was recently discussed using dynamical mean-field theory.[26] Using the similar parameters (Hubbard $U=0.2$ Ry, $J=0.06$ Ry) we have evaluated T_C for NiMnSb using the LSDA+U approach[27] and obtained $T_C=810$ K in the RPA (the FM reference state, all sublattices included). This temperature agrees with the experiment slightly better as compared to the LSDA value, but one should be cautious because of the uncertainty in the Hubbard U. In Fig. 5(b) we compare exchange interactions $J^{\mathrm{Mn,Mn}}$ and $J^{\mathrm{Mn,Ni}}$ evaluated in the LSDA and LSDA+U. While the nearest neighbor $J^{\mathrm{Mn,Mn}}$ is larger in the LSDA+U as compared to LSDA, the net effect is a lowering of T_C due to the next antiferromagnetic (AFM) couplings with larger shell numbers.

The FM and DLM reference states differ in the amount of spin correlations; the FM state is fully correlated while there are no spin correlations in the DLM state. The DLM reference state in general leads to slightly different electron occupations of majority and minority bands and, in turn, also to different Fermi surfaces, exchange parameters, and critical temperatures. Despite the fact that these changes are small, they influence exchange interactions in all shells and their

effect on T_C may not be negligible. As seen from Table II, the DLM state, with a higher total energy as compared to the FM state, enhances T_C. In some cases—e.g., for bcc Fe—such a choice leads to very good agreement with the experiment.[10]

The last effect which can influence the value of T_C is the electronic entropy. The mapping is done for $T=0$ while, strictly speaking, it should be done for $T=T_C$ by introducing the Fermi-Dirac function into Eq. (2). Preliminary tests indicate a negligible effect on T_C for $T \leqslant 500$ K while for $T \geqslant 1000$ K corresponding changes, which lower estimated T_C, could amount to tens of K. The strength of this influence increases with temperature.

IV. CONCLUSIONS

In conclusion, we have calculated magnetic moments and exchange interactions of Heusler alloys $Ni_{2-x}MnSb$ and estimated the corresponding Curie temperatures using the MFA, RPA (renormalized RPA), and MCS approaches applied here to the case of complex lattices with a few sublattices. We have also discussed the effect of pressure on exchange interactions and critical temperatures. The present study demonstrates good quantitative agreement of the calculated and experimental Curie temperatures for this alloy system evaluated using the RPA (renormalized RPA) and MCS approaches while the MFA overestimates critical temperatures and was found to be inaccurate for reliable quantitative estimates of T_C for magnetic materials with well-localized magnetic moments. Its success in particular cases[5,11,12] is to some extent fortuitous. We have also presented a detailed analysis of exchange interactions in the $Ni_{2-x}MnSb$ family of Heusler alloys. The end-point members NiMnSb and Ni_2MnSb exhibit a strikingly different behavior: they are strongly damped with the distance between atoms for the half-metallic NiMnSb while a well-pronounced RKKY-type behavior is found for the metallic Ni_2MnSb with the crossover between these limits in random alloys. One can conclude that properties of $Ni_{2-x}MnSb$ Heusler alloys are controlled by the behavior of the minority electrons at the Fermi energy. We have also found a weak magnetic short-range order above the Curie temperature by evaluating the real-space spin-spin correlation function and related quantities. These results are similar to those found earlier in conventional transition-metal ferromagnets. Finally, the present results also indicate some sensitivity of the calculated exchange interactions and estimated critical temperatures to the details of the electronic structure calculations (the reference state used for mapping, the mapping itself, the electronic entropy effects, and the influence of electron correlations beyond the LSDA). This is understandable but it should be kept in mind when comparing the results of different approaches in detail with the aim of finding the theoretical "error bar" for each specific magnetic system.

ACKNOWLEDGMENTS

J.R. and I.T. acknowledge financial support from the research program of the Ministry of Education of the Czech Republic (Grant No. MSM 0021620834). J.R. also acknowledges support from Project No. AVOZ10100521 of the Institute of Physics, Prague. J.K. and I.T. acknowledge financial support from Grant No. AVOZ10100520, the Grant Agency of the Academy of Sciences of the Czech Republic (Grant No. A100100616), and the Czech Science Foundation (Grant No. 202/04/0583). L.B. acknowledges support from the Swedish Natural Science Foundation (VR), the Swedish Foundation for Strategic Research (SSF), Seagate Inc., the National Supercomputer Centre (NSC), and High Performance Computing Center North (HPC2N).

*Electronic address: rusz@mag.mff.cuni.cz

†Also at Institute of Physics, Academy of Sciences of the Czech Republic, Cukrovarnická 10, 162 53, Prague 6, Czech Republic.

‡Also at Institute of Physics of Materials, Academy of Sciences of the Czech Republic, Brno, Czech Republic.

[1] P. Hohenberg and W. Kohn, Phys. Rev. **136**, B864 (1964); W. Kohn and L. J. Sham, Phys. Rev. **140**, A1133 (1965).

[2] A. I. Liechtenstein, M. I. Katsnelson, V. P. Antropov, and V. A. Gubanov, J. Magn. Magn. Mater. **67**, 65 (1987).

[3] V. P. Antropov, B. N. Harmon, and A. N. Smirnov, J. Magn. Magn. Mater. **200**, 148 (1999).

[4] M. Pajda, J. Kudrnovský, I. Turek, V. Drchal, and P. Bruno, Phys. Rev. B **64**, 174402 (2001).

[5] E. Sasioglu, L. M. Sandratskii, and P. Bruno, Phys. Rev. B **70**, 024427 (2004).

[6] L. M. Sandratskii and P. Bruno, Phys. Rev. B **67**, 214402 (2003).

[7] L. M. Sandratskii, Phys. Rev. B **68**, 224432 (2003).

[8] L. Bergqvist, O. Eriksson, J. Kudrnovský, V. Drchal, P. Korzhavyi, and I. Turek, Phys. Rev. Lett. **93**, 137202 (2004).

[9] J. Kudrnovský, I. Turek, V. Drchal, F. Máca, P. Weinberger, and P. Bruno, Phys. Rev. B **69**, 115208 (2004).

[10] A. V. Ruban, S. Shallcross, S. I. Simak, and H. L. Skriver, Phys. Rev. B **70**, 125115 (2004).

[11] Y. Kurtulus, R. Dronskowski, G. D. Samolyuk, and V. P. Antropov, Phys. Rev. B **71**, 014425 (2005).

[12] E. Sasioglu, L. M. Sandratskii, and P. Bruno, Phys. Rev. B **71**, 214412 (2005).

[13] E. Sasioglu, L. M. Sandratskii, and P. Bruno, J. Magn. Magn. Mater. **290–291**, 385 (2005).

[14] B. L. Gyorffy, A. J. Pindor, J. Staunton, G. M. Stocks, and H. Winter, J. Phys. F: Met. Phys. **15**, 1337 (1985).

[15] V. P. Antropov, J. Magn. Magn. Mater. **262**, L192 (2003).

[16] J. Rusz, I. Turek, and M. Diviš, Phys. Rev. B **71**, 174408 (2005).

[17] I. Turek, V. Drchal, J. Kudrnovský, M. Šob, and P. Weinberger, *Electronic Structure of Disordered Alloys, Surfaces and Interfaces* (Kluwer, Boston, 1997).

[18] P. J. Webster and R. M. Mankinar, J. Magn. Magn. Mater. **42**, 300 (1984).

[19] N. Majlis, *The Quantum Theory of Magnetism* (World Scientific, Singapore, 2001).

[20] Ya. G. Sinai, *Theory of Phase Transitions: Rigorous Results* (Pergamon Press, Oxford, 1982).
[21] D. P. Landau and K. Binder, *A Guide to Monte Carlo Simulations in Statistical Physics* (Cambridge University Press, Cambridge, England, 2000).
[22] P. Bruno, Phys. Rev. Lett. **90**, 087205 (2003).
[23] A. G. Gavriliuk, G. N. Stepanov, V. A. Sidorov, and S. M. Irkaev, J. Appl. Phys. **79**, 2609 (1995).
[24] S. Khmelevskyi, J. Kudrnovský, B. L. Gyorffy, P. Mohn, V. Drchal, and P. Weinberger, Phys. Rev. B **70**, 224432 (2004).
[25] S. V. Halilov, H. Eschrig, A. Y. Perlov, and P. M. Oppeneer, Phys. Rev. B **58**, 293 (1998).
[26] L. Chioncel, M. I. Katsnelson, R. A. de Groot, and A. I. Lichtenstein, Phys. Rev. B **68**, 144425 (2003).
[27] A. B. Shick, J. Kudrnovský, and V. Drchal, Phys. Rev. B **69**, 125207 (2004).
[28] N. M. Rosengaard and B. Johansson, Phys. Rev. B **55**, 14975 (1997).